Detection of inflamed atherosclerotic lesions with diadenosine-5′,5‴-P^1,P^4-tetraphosphate (Ap_4A) and positron-emission tomography

D. R. Elmaleh*†, A. J. Fischman*, A. Tawakol‡, A. Zhu*, T. M. Shoup*, U. Hoffmann*, A.-L. Brownell*, and P. C. Zamecnik§¶

*Department of Radiology and ‡Cardiology Division, Massachusetts General Hospital, Boston, MA 02114; and §Department of Medicine, Massachusetts General Hospital, Charlestown, MA 02129

Contributed by P. C. Zamecnik, August 24, 2006

Diadenosine-5′,5‴-P^1,P^4-tetraphosphate (Ap_4A) and its analog P^2,P^3-monochloromethylene diadenosine-5′,5‴-P^1,P^4-tetraphosphate (AppCHClppA) are competitive inhibitors of adenosine diphosphate-induced platelet aggregation, which plays a central role in arterial thrombosis and plaque formation. In this study, we evaluate the imaging capabilities of positron-emission tomography (PET) with P^2,P^3-[^{18}F]monofluoromethylene diadenosine-5′,5‴-P^1,P^4-tetraphosphate ([^{18}F]AppCHFppA) to detect atherosclerotic lesions in male New Zealand White rabbits. Three to six months after balloon injury to the aorta, the rabbits were injected with [^{18}F]AppCHFppA, and microPET imaging showed rapid accumulation of this radiopharmaceutical in the atherosclerotic abdominal aorta, with lesions clearly visible 30 min after injection. Computed tomographic images were coregistered with PET images to improve delineation of aortoiliac tracer activity. Plaque macrophage density, quantified by immunostaining with RAM11 against rabbit macrophages, correlated with PET measurements of [^{18}F]AppCHFppA uptake ($r = 0.87$, $P < 0.0001$), whereas smooth-muscle cell density, quantified by immunostaining with 1A4 against smooth muscle actin, did not. Biodistribution studies of [^{18}F]AppCHFppA in normal rats indicated typical adenosine dinucleotide behavior with insignificant myocardial uptake and fast kidney clearance. The accumulation of [^{18}F]AppCHFppA in macrophage-rich atherosclerotic plaques can be quantified noninvasively with PET. Hence, [^{18}F]AppCHFppA holds promise for the noninvasive characterization of vascular inflammation.

atherosclerosis | vascular damage | plaque imaging

Our previous findings with ^{99m}Tc-conjugated diadenosine-5′,5‴-P^1,P^4-tetraphosphate (Ap_4A) and P^2,P^3-monochloromethylene diadenosine-5′,5‴-P^1,P^4-tetraphosphate (AppCHClppA) in a rabbit model indicated rapid, high accumulation of both diadenosine tetraphosphate analogs in the atherosclerotic abdominal aorta and demonstrated up-regulation of purine receptors in experimental atherosclerotic lesions, suggesting the potential for using such labeled analogs for noninvasive detection of plaque formation (1, 2). The atherogenic process involves sequestration of partially oxidized lipids in the vessel wall (3, 4), leading to endothelial injury that promotes adherence of mononuclear cells and platelets and contributes to phenotypic transformation of medial smooth muscle cells (SMCs) from adult to embryonic forms. The transformed muscle cells proliferate and migrate to the intima in parallel with accumulation of lipids by monocytes, causing the formation of foam cells. Other processes of plaque formation, involving T lymphocytes, platelets, cytokine release, and growth factors, enhance migration and proliferation of SMCs (3–7). Vulnerable plaque formation is associated with increased monocyte/macrophage representation and arterial wall cap thinning. Plaque disruption is the major event for inducing thrombosis and acute coronary syndromes (8).

Evidence indicates an important role for adenosine nucleotides in the development of atherosclerotic plaque inflammation.

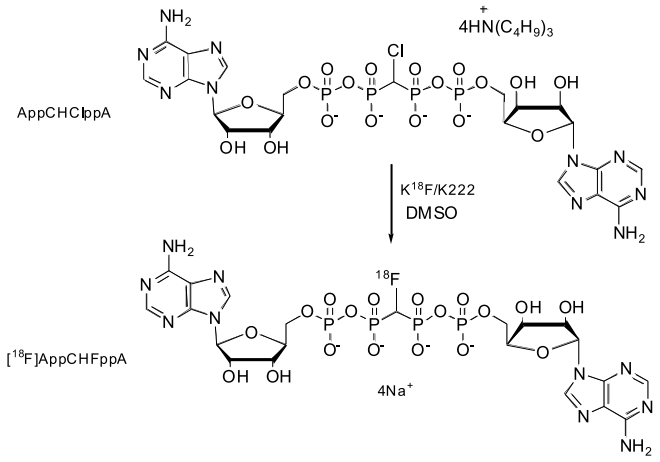

Fig. 1. Formulae for monochloro- and monofluoro-Ap_4A.

Extracellular adenosine nucleotides are released from a variety of cells and regulate many physiologic activities by interaction with P2 receptors or adenosine nucleotide receptors (9–12). The development of atherosclerosis is closely associated with up-regulation of the extracellular purinergic receptor $P2Y_2R$, whose activation in vascular endothelial cells induces expression of vascular cell adhesion molecule 1 (VCAM-1) and adherence of monocytes, as well as the release of proinflammatory chemokines (13).

Molecular imaging probes and techniques based on intravascular MRI, computed tomography (CT), ultrasound, and optical coherence tomography have been proposed for accurate identification of atherosclerotic plaque, plaque formation, and vul-

Author contributions: D.R.E., A.J.F., A.T., and P.C.Z. designed research; D.R.E., A.T., A.Z., T.M.S., and A.-L.B. performed research; U.H. contributed new reagents/analytic tools; D.R.E. and P.C.Z. analyzed data; D.R.E. and P.C.Z. wrote the paper; A.Z. and A.-L.B. performed PET imaging; T.M.S. performed radiochemical preparation; and U.H. performed CT imaging.

Conflict of interest statement: D.R.E. and P.C.Z. are coinventors on a patent held by Massachusetts General Hospital on radionuclide imaging of Ap_4A and certain analogs in cardiovascular disease, licensed to Fluoropharma, Inc. D.R.E. is a member of the Board of Directors of Fluoropharma, Inc.

Freely available online through the PNAS open access option.

Abbreviations: AppCHClppA, P^2,P^3-monochloromethylene diadenosine-5′,5‴-P^1,P^4-tetraphosphate; Ap_4A, diadenosine-5′,5‴-P^1,P^4-tetraphosphate; CT, computed tomography; [^{18}F]AppCHFppA, P^2,P^3-[^{18}F]monofluoromethylene diadenosine 5′,5‴-P^1,P^4-tetraphosphate; PET, positron-emission tomography; SMC, smooth muscle cell.

†To whom correspondence may be addressed at: Division of Nuclear Medicine, Massachusetts General Hospital, 55 Fruit Street, Boston, MA 02114. E-mail: delmaleh@partners.org.

¶To whom correspondence may be addressed at: Massachusetts General Hospital, MC 1494005, 149 13th Street, Charlestown, MA 02129-2000.

www.pnas.org/cgi/doi/10.1073/pnas.0607246103

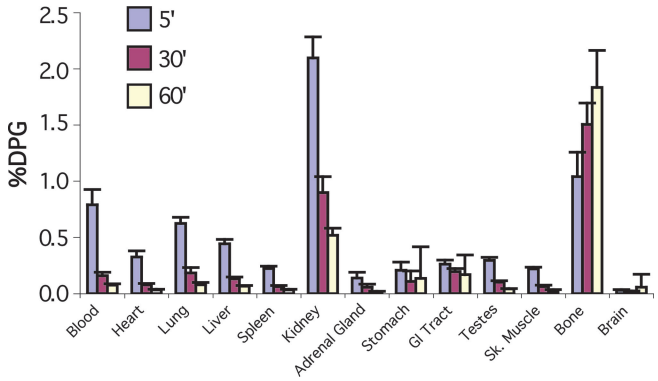

Fig. 2. [^{18}F]AppCHFppA rat biodistribution. Note the decrease in concentration of radioactivity with time in kidney and increase with time in bone. If the concentration in bone represents intact compound, it may prove to be a useful marker. %DPG, percentage injected dose per gram.

nerable plaque. Most approaches are invasive, and none have demonstrated the diagnostic accuracy necessary to replace invasive angiography (3, 14–22). A limited number of reports describe noninvasive visualization of atherosclerotic lesions. These studies have targeted the thrombotic component overlying the atherosclerotic lesion (with radiolabeled fibrinogen) (23, 24), platelet aggregation at regions of turbulent flow (with labeled platelets or platelet-specific antibodies) (25, 26), and proteins likely to be incorporated into atherosclerotic lesions (with radiolabeled autologous lipoproteins). Nonspecific uptake of human IgG by Fc receptors on macrophages has also formed the basis of a targeting strategy (27). More recently, the F(ab′) fragments of monoclonal IgM antibody Z2D3, which was initially developed with specificity for an antigen expressed by proliferating SMCs of human atherosclerotic lesions, have demonstrated rapid accumulation and good localization of lesions in an experimental atherosclerotic model (28–29). Fluorine-18-labeled fluorodeoxyglucose has also been used for imaging of carotid artery plaque (30–31).

We have shown rapid and high accumulation of ^{99m}Tc-conjugated by chelation adenosine nucleotide polyphosphates in inflamed atherosclerotic plaques (2). In addition, a closely related analog, P^2,P^3-mono[^{18}F]fluoromethylene diadenosine-5′,5‴-P^1,P^4-tetraphosphate ([^{18}F]AppCHFppA), which is an ^{18}F-labeled molecular probe (9), may be preferable because it is more securely attached by covalent linkage to the parent compound and accumulates selectively in atherosclerotic lesions, thereby allowing the noninvasive characterization of plaque inflammation with positron-emission tomography (PET) imaging. Such a method could be important not only for diagnosis but also for the development and monitoring of therapies directed at altering the natural history of these lesions.

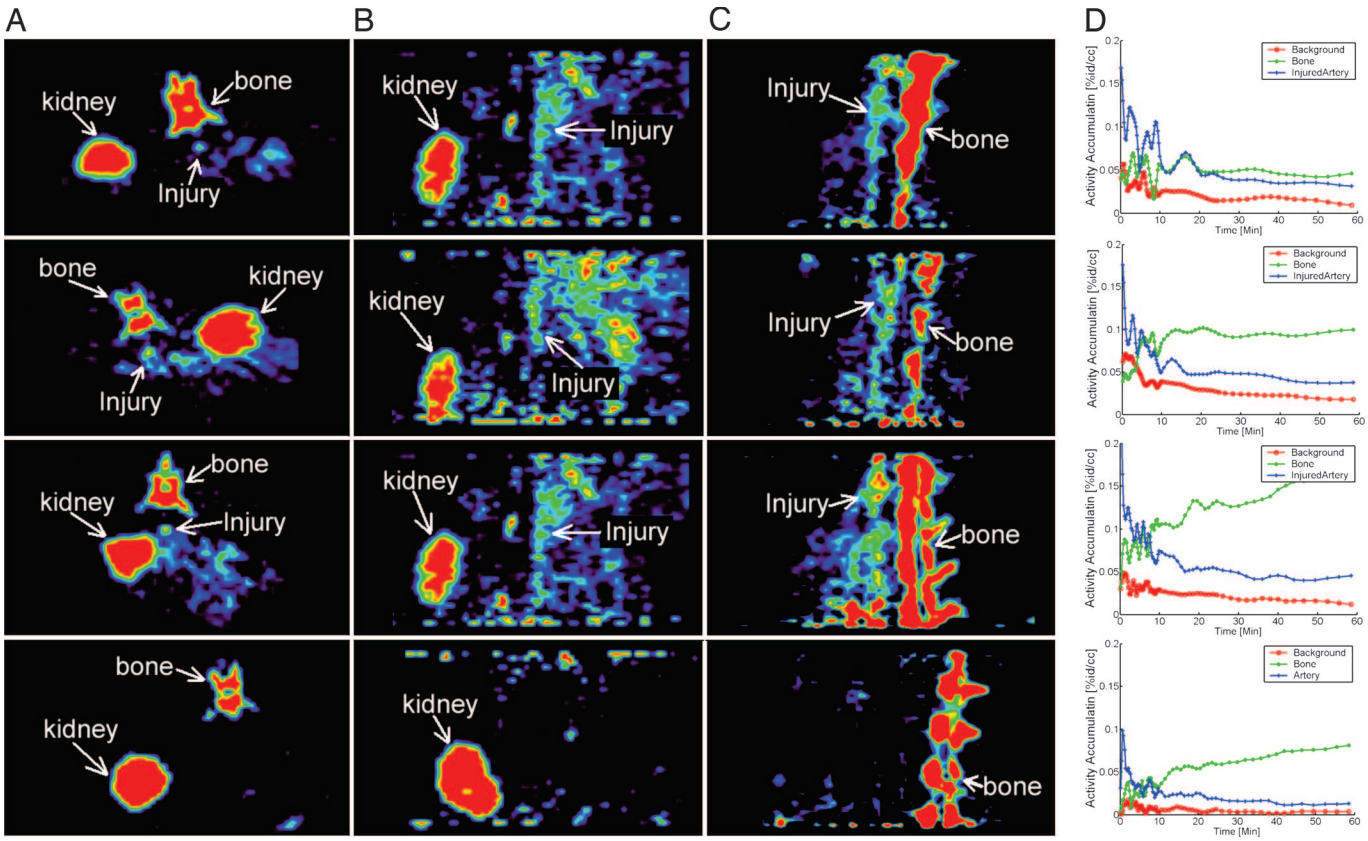

Fig. 3. MicroPET images of the aorta acquired in the experimental atherosclerotic rabbit model (first through third rows) and in the normal control rabbit (fourth row) 30 min after injection of [^{18}F]AppCHFppA (111 MBq) in an ear vein. Three-dimensional dynamic data were acquired in list mode for 1 h starting from the injection of the radiolabeled ligand. PET imaging studies were conducted with a microPET P4 system (Concorde Microsystems, Knoxville, TN). First through third rows, atherosclerotic rabbit model with activity distribution in (*A*) transverse view, (*B*) axial view, and (*C*) sagittal view, showing accumulation of radiopharmaceutical in injured artery and spine, and (*D*) time–activity curves indicating that the injured artery (blue) has enhanced accumulation compared with background (yellow). Fourth row, normal rabbit with activity distribution showing lack of accumulation of radiopharmaceutical in (*A*) transverse view, (*B*) axial view, and (*C*) sagittal view, and (*D*) time–activity curve of the radiopharmaceutical in artery (pink) and bone (blue). %id/cc, percentage injected dose per cubic centimeter.

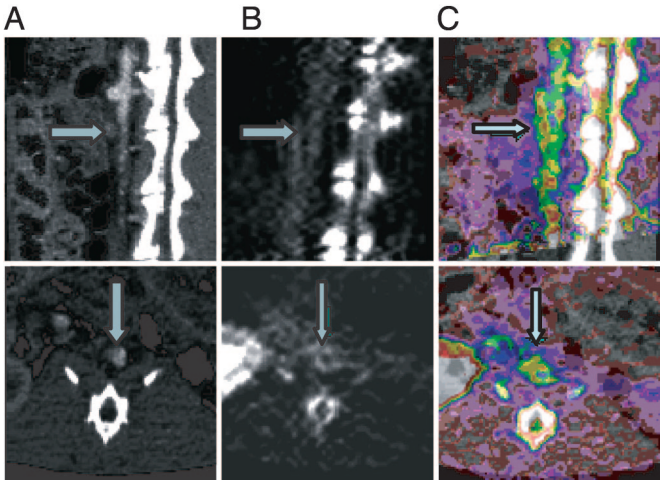

Fig. 4. Coregistration of CT and PET images. CT images (*A*) and PET images (*B*) were coregistered (*C*) by employing a workstation (REVEAL-MVS) that enables multimodal standard (rigid) image fusion using anatomic landmarks. After PET scanning, CT angiography was performed with a Siemens Medical Solutions SOMATOM Sensation 16-slice CT scanner (Siemens Systems, Forcheim, Germany). Three-dimensional, multiplanar reconstruction of raw images was performed, and the CT images were then coregistered with the PET images. With the CT/PET image as a guide, region-of-interest segments of the thoracic and abdominal aorta were drawn. Accumulation of radioactivity was calculated for each region of interest and expressed as percentage injected dose per milliliter. A value of $P < 0.05$ was considered significant. *Upper* row, sagittal sections; *Lower* row, transverse sections. Arrows in *A* indicate lumen with CT contrast; arrows in *B* indicate arterial wall plaque; and arrows in *C* show the fusion of lumen CT contrast in wall plaque in the PET image.

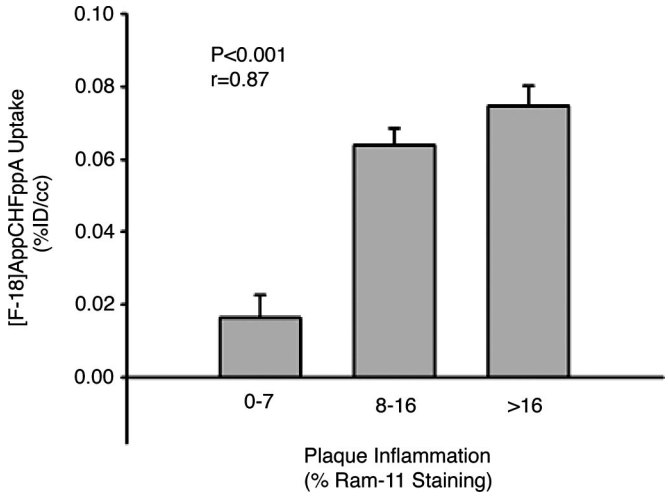

Fig. 5. Noninvasive (PET) measurements of [^{18}F]AppCHFppA uptake correlated with macrophage density (percentage macrophage staining), assessed by staining with mAb against rabbit macrophages (RAM11) ($r = 0.87$, $P < 0.0001$). %ID/cc, percentage injected dose per cubic centimeter.

Results and Discussion

AppCHClppA was prepared as described previously (32). No-carrier-added radiofluorination of tetra(tributylammonium) salt with [^{18}F]fluoride was effected by nucleophilic substitution (Fig. 1) under anhydrous conditions to afford [^{18}F]AppCHFppA with yields between 20% and 40%.

A biodistribution study of [^{18}F]AppCHFppA in rats indicated behavior typical of adenine dinucleotides, with minimal myocardial uptake and fast kidney washout (see Fig. 2). The accumulation (percentage of injected dose per gram) in most normal tissues was low: blood (0.78%, 0.16%, and 0.07%), heart (0.33%, 0.08%, and 0.03%), lung (0.62%, 0.18%, and 0.08%), liver (0.33%, 0.08%, and 0.03%), and kidney (2.10%, 0.90%, and 0.03%) at 5, 30, and 60 min, respectively. Bone accumulation (1.04%, 1.51%, and1.83%) may be a result of defluorination and/or tetraphosphonate bone uptake. Of all the tissues sampled, kidney contained the highest early concentration of tracer ($P < 0.01$); liver and lung had higher concentrations than spleen and muscle ($P < 0.05$); and spleen accumulation was similar to that in muscle ($P < 0.05$).

To assess the ability of [^{18}F]AppCHFppA to target inflamed atherosclerotic plaques, we acquired microPET images (see *Materials and Methods*) in a rabbit model of experimental atherosclerosis, with aortoiliac endothelial denudation achieved using a modified Baumgartener technique (33). In Fig. 3, the first through third rows contain 30-min transverse (*A*), axial (*B*), and sagittal (*C*) images from three rabbits in which the lesioned aorta is clearly visualized. The lesions can be seen within 10 min after radiopharmaceutical injection, and radioactivity is retained for the 1-h imaging session. Blood clearance of the radiopharmaceutical is rapid (Fig. 2). The lesion-to-blood radioactivity ratio at 1 h is >5:1. Time–activity curves indicate that the injured artery has enhanced accumulation compared with the background (Fig. 3*D*). In control animals (Fig. 3, fourth row), there is little or no significant accumulation of the radiopharmaceutical in aortic tissues. Because of the three-dimensional, high-resolution capability of PET, bone accumulation is not a crucial factor in the use of the proposed probe. CT images obtained by multimodal standard (rigid) image fusion (REVEAL-MVS workstation; Mirada Solutions, Oxford, U.K.) using anatomic landmarks (Fig. 4) confirm these findings. The coregistration clearly shows the fusion of the lumen border into the plaque (arrow) in the PET image activity.

In addition, microPET images correlate with *ex vivo* pathology data (quantitative histomorphometry performed by a blinded observer, with digital planimetric determination of intimal and medial areas on a representative cross-section of each arterial segment) and with areas of atherosclerosis identified by histology [inflammation quantified by using planimetry, and macrophage density (percentage macrophage staining) calculated as reported previously (33)]. For immunohistochemistry studies, aortic specimens were stained with mAb against rabbit macrophage (RAM11; Dako, Carpinteria, CA) (Fig. 5) and smooth muscle actin (1A4; Dako); [^{18}F]AppCHFppA uptake is associated with macrophage density ($r = 0.87$, $P < 0.0001$; Fig. 5) but not with SMC number ($r = 0.26$, $P = 0.40$). These findings suggest the feasibility of instant noninvasive imaging of experimentally induced atherosclerotic lesions with radiolabeled [^{18}F]AppCHFppA.

Adenosine nucleotides are involved in active inhibition of platelet aggregation and, therefore, exhibit high affinity to platelets by means of their binding to the platelet P2T receptors and specific oligonucleotide receptors (10). Adenine nucleotides are capable of extensive binding to the metabotropic P2Y receptors and the transmitter-gated ion channel P2X receptors, which are augmented in atherosclerosis due to the increased population of macrophages and monocytes. These oligonucleotides are promising, offering more specific receptor sites, and yet are less studied than purinotropic receptors. Changes in the receptor sites of oligonucleotides are part of the pathogenesis of the atherosclerotic lesion process. The role of surface receptors coupled with intrinsic tyrosine kinase activity has been studied extensively in SMC proliferation in atheroma, but the role of G protein-coupled receptors (P2R) has not been described. The work described here provides *in vivo* characterization of the purine and oligonucleotide receptors in the ongoing vascular inflammation process.

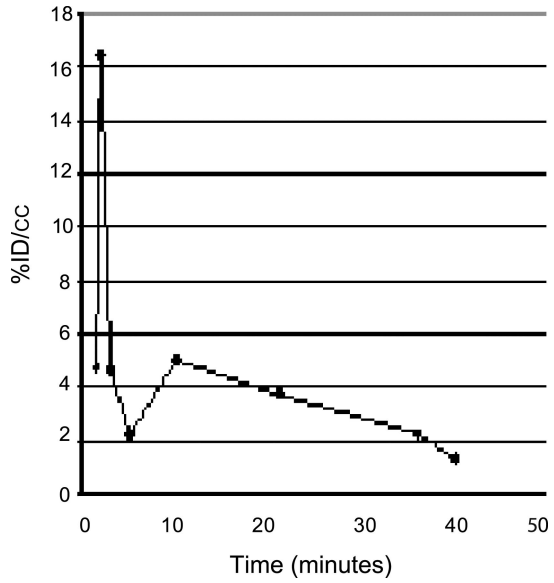

Fig. 6. Blood clearance evaluated during microPET imaging by sampling the blood at various times (1–40 min) and calculating the percentage of injected dose per cubic centimeter.

Although the clinical diagnostic method for detecting atherosclerotic lesions measures the extent of luminal narrowing, thus providing a basis for therapeutic intervention, it does not preclude poor prognostic outcomes in cases of milder degrees of narrowing. For optimal care of atherosclerotic disease, characterization of plaque constitution is imperative. It will be useful to predict whether the plaque is likely to rupture or impinge on the lumen rapidly or to progress slowly with stable surface characteristics. Quantitative differentiation among the foam cell-rich lesions, high-proliferating SMC index, and the amount of overlying thrombotic plaque will affect prognostication. Because the uptake of [^{18}F]AppCHFppA is rapid, plaque imaging can be recorded earlier than when using IK17 mAb specific for an oxidized low-density lipoprotein (2) or Z2D3 mAb specific for proliferating SMCs (27). Various clinical vasculopathies associated with rapid proliferation of SMCs include restenotic complications of angioplastic interventions and allograft-related vasculopathy. Neither diagnostic nor prognostic strategies have provided sufficient information to permit early intervention in these cases. It is expected that determination of an independent index of both purine and oligonucleotide receptor up-regulation and increased macrophage concentration will provide sensitive markers for prediction.

Conclusions

These studies demonstrate that quantifying the up-regulation of purine and specific oligonucleotide receptors in atherosclerotic lesions by using labeled adenosine oligonucleotides such as [^{18}F]AppCHFppA is a potential technique for noninvasive *in vivo* detection of plaque formation.

Materials and Methods

Synthesis of AppCHClppA (Labeling Precursor). AppCHClppA was prepared as described previously (32) and converted to the tributylammonium salt, which has better solubility than the sodium salt in organic solvents. This conversion was effected with Dowex 50W X-4 by ion exchange to the pyridinium salt, followed by treatment with tributylamine to give the tributylammonium salt.

Radiofluorination. [^{18}F]AppCHFppA was prepared from the AppCHClppA tetra(tributylammonium) salt and [^{18}F]fluoride by nucleophilic substitution (Fig. 1). A Wheaton 5-ml reaction vial containing fluorine-18 (3.7 GBq, 100 mCi) in ^{18}O-enriched water (0.5 ml), Kryptofix 222 (8 mg; Aldrich, Milwaukee, WI), and potassium carbonate (2 mg) was heated at 115°C, and solvent was evaporated with the aid of nitrogen gas. The K^{18}F/Kryptofix complex was dried three times by the repetitive process of the addition of acetonitrile (1 ml) followed by evaporation of the solvent with a nitrogen flow. A solution of AppCHClppA (6 mg) in DMSO (400 μl) was added to the vial, and fluorination was performed at 120°C for 10 min. Once cooled to room temperature, the mixture was diluted with water (1 ml), and the solution was loaded onto a series of four C_{18} Sep-Pak columns (Waters, Milford, MA) connected in series. The columns were washed first with 20 mM PBS (10 ml, pH 7.2) to remove unreacted [^{18}F]fluoride and DMSO, and then the product was eluted using a mixture of acetonitrile: buffer solution (50:50, vol/vol). Acetonitrile in the fraction containing [^{18}F]AppCHFppA was removed by vacuum, and the final solution was filtered (0.22-μm MillexGV; Millipore, Billerica, MA). The product was obtained in 20–40% yield; radiochemical purity of the tracer for injection was 98% [specific activity > 185,000 GBq (5,000 Ci)/mmol].

Biodistribution in Rats. Male Sprague–Dawley rats (300–350 g; Charles River Breeding Laboratories, Preston, CT) were fasted overnight, and the animals were anesthetized with a mixture of ketamine (40–80 mg/kg and xylazine (5–10 mg/ml). Thereafter, [^{18}F]AppCHFppA (185 MBq/kg body weight) was administered, and the animals were killed with an overdose of sodium pentobarbital. Samples of blood, heart, lung, liver, spleen, kidney, adrenal gland, stomach, small intestine, skeletal muscle, and bone marrow were weighed, and radioactivity was assessed with a well-type gamma counter (model 1282; LKB, Mt. Waverley, Australia). Measurements for each specimen were recorded as cpm and corrected for background and radioactive decay. The concentration of radioactivity in each organ and fraction is expressed as percentage of injected dose per gram and percentage dose per organ (see Fig. 2). The extent of degradation of the intact labeled compound should be studied, particularly in kidney, bone marrow, and blood.

Experimental Atherosclerotic Lesions. Male New Zealand White rabbits weighing 2.5–3.0 kg (Charles River Breeding Laboratories) were maintained on a 2% cholesterol/6% peanut oil diet (ICN Biomedicals, Costa Mesa, CA) for 3–6 months. After 1 week of the hyperlipidemic diet, aortoiliac endothelial denudation was achieved by using a modified Baumgartener technique (33). Briefly, each animal was anesthetized with 1.5–2.0 ml s.c. of ketamine (100 mg/ml) and xylazine (100 mg/ml) mixed at 10:1 (vol/vol), and the right femoral artery was isolated. A 4F Fogarty embolectomy catheter (12–040-4F; Edwards Laboratories, Santa Ana, CA) was introduced through an arteriotomy and advanced to the level of the diaphragm. The catheter was inflated to a pressure of 3 psi above the balloon inflation pressure and withdrawn five times. The femoral artery was then ligated and the wound closed. After the rabbits recovered from anesthesia, they were returned to their cages and given a range of exposures to a high-cholesterol diet (3–6 months) to achieve varying degrees of atherosclerosis and inflammation. Untreated male New Zealand White rabbits fed standard chow served as controls. The protocol was approved by the Animal Care and Use Committee of Massachusetts General Hospital and complies with National Institutes of Health approved guidelines.

MicroPET Imaging of Atherosclerotic and Normal Rabbits. Before imaging, rabbits were anesthetized with ketamine/xylazine as

above. An ear vein was catheterized for administration of the radiolabeled ligand, and the body was wrapped with an underpad to maintain temperature. The rabbit was placed ventrally in the imaging position, and [^{18}F]AppCHFppA (111 MBq) was injected into the ear vein. During the imaging studies, blood clearance was evaluated by sampling the blood at various times (1–40 min) and counting the aliquots in a gamma counter (Fig. 6).

Three-dimensional dynamic data were acquired in list mode for 1 h beginning with injection of the radiolabeled ligand. PET imaging studies were conducted with a microPET P4 system (Concorde Microsystems, Knoxville, TN). The field of view was 8 cm, and the diameter was 22 cm, allowing imaging of the entire lower body of the rabbit in a single acquisition. The imaging parameters of this system were in plane with an axial resolution of 1.2 mm full width of photopeak measured at half maximal count. Before PET imaging, the animals were fixed to the imaging table with a custom-fabricated mold.

After PET scanning, CT angiography was performed using a Siemens Medical Solutions SOMATOM Sensation 16-slice CT scanner (Siemens Systems, Forcheim, Germany) with 0.75-mm slices in helical full-scan mode at a pitch of 2.8, tube voltage of 80 kV, and tube amperage of 35 mA. Initially, a scout topogram was obtained without contrast for purposes of orientation. A CT angiogram of the abdominal aorta was then acquired with automated i.v. injection of nonionic iodinated contrast (iodixanol) at a rate of 5 ml/sec. Three-dimensional multiplanar reconstruction of raw images was then undertaken. Subsequently, the CT images were coregistered with the PET images by employing a workstation (REVEAL-MVS) that enables multimodal standard (rigid) image fusion using anatomic landmarks. With the coregistered CT/PET image as a guide, region-of-interest segments of the thoracic and abdominal aorta were drawn. The accumulation of radioactivity was calculated for each region of interest and expressed as percentage of injected dose per cubic centimeter. Spatial resolution at the center of the imaging field was 1.8 mm. (The absolute activity values obtained from arteries and veins may be degraded due to the partial volume effect.)

Small sections were obtained from both lesional and normal aortic segments, fixed in buffered formaldehyde, and submitted for histologic examination.

Histopathology. Aortic and iliac specimens were fixed in phosphate-buffered formalin, embedded in paraffin, and stained with H&E and Masson's trichrome stains. Immunohistochemistry was performed using monoclonal antibodies against rabbit macrophages (RAM11) and smooth muscle actin (1A4). Quantitative histomorphometry was performed by a blinded observer, with digital planimetric determination of intimal and medial areas on a representative cross-section of each arterial segment. Inflammation was quantified by using planimetry, and macrophage density (percentage macrophage staining) was calculated as reported previously (34).

Statistical Methods. Data were analyzed using SPSS for Windows version 10.0 (SPSS, Chicago, IL). Gamma-counter measurements were related to histomorphometry findings for macrophage density by using Spearman's rank correlation method. For PET, standard uptake value data were correlated with CT image anatomy, with a value of $P < 0.05$ considered significant.

This work was supported in part by grants from The G. Harold and Leila V. Mathers Foundation and National Institutes of Health Grant 5 R01 AI060872–02 (to P.C.Z.).

1. Elmaleh DR, Zamecnik PC, Castronovo FP, Jr, Strauss HW, Rapaport E (1984) *Proc Natl Acad Sci USA* 81:918–921.
2. Elmaleh DR, Narula J, Babich JW, Petrov A, Fischman AJ, Khaw BA, Rapaport E, Zamecnik PC (1998) *Proc Natl Acad Sci USA* 95:691–695.
3. Tsimikas S (2002) *Am J Cardiol* 90:L22–L27.
4. Ross R (1986) *N Engl J Med* 314:488–500.
5. Grotendorst GR, Seppa HEJ, Kleinman HK, Martin GR (1981) *Proc Natl Acad Sci USA* 78:3669–3672.
6. Thyberg J, Hedin U, Sjolund M, Palmberg L, Bottger BA (1990) *Arteriosclerosis* 10:966–990.
7. Butcher EC (1991) *Cell* 67:1033–1036.
8. Seshiah PN, Kereiakes DJ, Vasudevan SS, Lopes N, Su BY, Flavahan NA, Goldschmidt-Clermont PJ (2002) *Circulation* 105:174–180.
9. Zamecnik PC, Kim B, Guo MJ, Taylor G, Blackburn GM (1992) *Proc Natl Acad Sci USA* 89:2370–2373.
10. Boeynaems, J-M, Communi D, Gonzalez NS, Robaye B (2005) *Semin Thromb Hemostasis* 31:139–149.
11. Yaar R, Jones MR, Chen J-F, Ravid K (2005) *J Cell Physiol* 202:9–20.
12. Sands WA, Palmer TM (2005) *Immunol Lett* 101:1–11.
13. Cox MA, Gomes B, Palmer K, Du K, Wiekowski M, Wilburn B, Petro M, Chou C-C, Desquitado C, Schwarz M, *et al.* (2005) *Biochem Biophys Res Commun* 330:467–473.
14. Callister TQ, Cooil B, Raya SP, Lippolis NJ, Russo DJ, Raggi P (1998) *Radiology* 208:807–814.
15. Toussaint JF, Pachot-Clouard M, Bridal SL, Gouya H, Berger G (1999) *Arch Mal Coeur Vaiss* 92:349–354.
16. Nissen SE, Yock P (2001) *Circulation* 103:604–616.
17. Patwari P, Weissman NJ, Boppart SA, Jesser C, Stamper D, Fujimoto JG, Brezinski ME (2000) *Am J Cardiol* 85:641–644.
18. Weissleder R, Mahmood U (2001) *Radiology* 219:316–333.
19. Fayad ZA, Fuster V, Nikolaou K, Becker C (2002) *Circulation* 106:2026–2034.
20. Aime S, Cabella C, Colombatto S, Geninatti C, Gianolio E, Maggioni F (2002) *J Magn Reson Imaging* 16:394–406.
21. Wickline SA, Lanza GM (2003) *Circulation* 107:1092–1095.
22. Kooi ME, Cappendijk VC, Cleutjens KB, Kessels AGH, Kitslaar PJ, Borgers M, Frederik PM, Daemen MJAP, van Engelshoven JMA (2003) *Circulation* 107:2453–2458.
23. Mettinger KL, Larson S, Ericson K, Casseborn S (1978) *Lancet* 1:242–244.
24. Ord JM, Hasapes J, Daugherty A, Thorpe SR, Bergmann SR, Sobel BE (1992) *Circulation* 85:288–297.
25. Davis HH, Siegel BA, Sherman LA, Heaton WA, Naidich TP, Joist JH, Welch MJ (1980) *Circulation* 61:982–988.
26. Minar E, Ehringer H, Dudczak R, Schofl R, Jung M, Koppensteiner R, Ahmadi R, Kretschmer G (1989) *Stroke* 20:27–33.
27. Fischman AJ, Rubin RH, Delvecchio A, Ahmad M, Khaw BA, Callahan RJ, LaMuraglia GM, Strauss HW (1989) *J Nucl Med* 30:817–820.
28. Narula J, Petrov A, Bianchi C, Ditlow CC, Lister BC, Dilley J, Pieslak I, Chen FW, Torchilin VP, Khaw BA (1995) *Circulation* 92:474–484.
29. Khaw BA, Carrio J, Narula J (1995) *Handbook of Targeted Delivery of Imaging Agents* (CRC Press, Boca Raton, FL), pp 429–443.
30. Lederman RJ, Raylman RR, Fisher SJ, Kison PV, San H, Nabel EG, Wahl RL (2001) *Nucl Med Commun* 22:747–753.
31. Rudd JHF, Warburton EA, Fryer TD, Jones HA, Clark JC, Antoun N, Johnstrom P, Davenport AP, Kirkpatrick PJ, Arch, BN, *et al.* (2002) *Circulation* 105:2708–2711.
32. Blackburn GM, Guo M-J, McLennan AG (1992) in *Ap$_4$A and Other Dinucleoside Polyphosphates*, ed McLennan AG (CRC Press, Boca Raton, FL), pp 305–342.
33. Baumgartener HR (1963) *Z Gesamte Exp Med* 137:227–249.
34. Jander S, Sitzer M, Schumann R, Schroeter M, Siebler M, Steinmetz H, Stoll G (1998) *Stroke* 29:1625–1630.